

**Journal of Materials Chemistry A**  
Supplementary Information

**Reduction on reactive pore surface as a versatile approach to monolith-supported metal alloy nanoparticles and its catalytic applications**

Nirmalya Moitra, Kazuyoshi Kanamori,\* Yumi H. Ikuhara, Xiang Gao, Yang Zhu, George Hasegawa, Kazuyuki Takeda, Toyoshi Shimada and Kazuki Nakanishi\*

**Table S1** Starting compositions for mono- and multi-metallic nanoparticles

Sample <sup>a</sup>	HAuCl <sub>4</sub> /mmol	PdCl <sub>2</sub> /mmol	H <sub>2</sub> PtCl <sub>6</sub> /mmol	RhCl <sub>3</sub> /mmol	Average Particle Size/nm
Au	0.040				38 <sup>b</sup>
Pd		0.040			25 <sup>b</sup>
Pt			0.040		6 <sup>b</sup>
Rh				0.040	7 <sup>b</sup>
Au <sub>4</sub> Pd <sub>1</sub>	0.032	0.008			
Au <sub>3</sub> Pd <sub>1</sub>	0.030	0.010			27 <sup>c</sup>
Au <sub>2</sub> Pd <sub>1</sub>	0.027	0.013			
Au <sub>1</sub> Pd <sub>1</sub>	0.020	0.020			12 <sup>c</sup>
Au <sub>1</sub> Pd <sub>2</sub>	0.013	0.027			
Au <sub>1</sub> Pd <sub>3</sub>	0.010	0.030			6 <sup>c</sup>
Au <sub>1</sub> Pd <sub>4</sub>	0.008	0.032			
Au <sub>4</sub> Pt <sub>1</sub>	0.032		0.008		
Au <sub>3</sub> Pt <sub>1</sub>	0.030		0.010		
Au <sub>2</sub> Pt <sub>1</sub>	0.027		0.013		
Au <sub>1</sub> Pt <sub>1</sub>	0.020		0.020		6 <sup>c</sup>
Au <sub>1</sub> Pt <sub>2</sub>	0.013		0.027		
Au <sub>1</sub> Pt <sub>3</sub>	0.010		0.030		
Au <sub>1</sub> Pt <sub>4</sub>	0.008		0.032		
Pd <sub>4</sub> Rh <sub>1</sub>			0.032	0.008	
Pd <sub>3</sub> Rh <sub>1</sub>			0.030	0.010	
Pd <sub>2</sub> Rh <sub>1</sub>			0.027	0.013	
Pd <sub>1</sub> Rh <sub>1</sub>			0.020	0.020	6 <sup>c</sup>
Pd <sub>1</sub> Rh <sub>2</sub>			0.013	0.027	
Pd <sub>1</sub> Rh <sub>3</sub>			0.010	0.030	
Pd <sub>1</sub> Rh <sub>4</sub>			0.008	0.032	
Pt <sub>4</sub> Rh <sub>1</sub>		0.032		0.008	
Pt <sub>3</sub> Rh <sub>1</sub>		0.030		0.010	
Pt <sub>2</sub> Rh <sub>1</sub>		0.027		0.013	
Pt <sub>1</sub> Rh <sub>1</sub>		0.020		0.020	4 <sup>c</sup>
Pt <sub>1</sub> Rh <sub>2</sub>		0.013		0.027	
Pt <sub>1</sub> Rh <sub>3</sub>		0.010		0.030	
Pt <sub>1</sub> Rh <sub>4</sub>		0.008		0.032	
Au <sub>1</sub> Pd <sub>1</sub> Pt <sub>1</sub>	0.013	0.013	0.013		13 <sup>c</sup>
Au <sub>1</sub> Pd <sub>1</sub> Rh <sub>1</sub>	0.013	0.013		0.013	242 <sup>c</sup>
Au <sub>1</sub> Pt <sub>1</sub> Rh <sub>1</sub>	0.013		0.013	0.013	6 <sup>c</sup>
Pd <sub>1</sub> Pt <sub>1</sub> Rh <sub>1</sub>		0.013	0.013	0.013	8 <sup>c</sup>
Au <sub>1</sub> Pd <sub>1</sub> Pt <sub>1</sub> Rh <sub>1</sub>	0.010	0.010	0.010	0.010	309 <sup>c</sup>

<sup>a</sup>HSQ = 53 mg (1 mmol); metal(s) = 0.04 mmol; water = 1.0 mL; acetone = 19 mL; time = 36 h; temperature = 50 °C

<sup>b</sup>Average particle size derived from XRD by the Scherrer's equation.

<sup>c</sup>Average particle size derived from HAADF-STEM images.

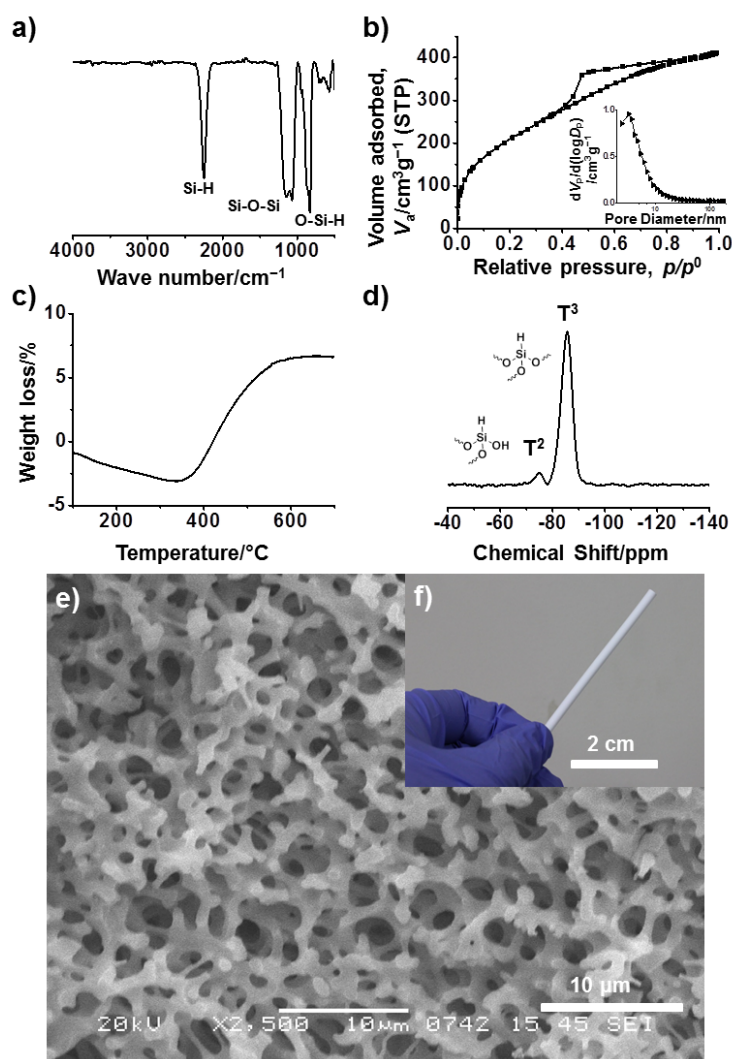


**Figure S1** (a) FT-IR spectrum of the HSQ monolith, showing Si-H, O-Si-H and Si-O-Si characteristic absorptions. (b) Nitrogen adsorption-desorption isotherm (BET specific surface area = 800 m<sup>2</sup>/g) and BJH mesopore size distribution plot derived from adsorption branch of the isotherm (inset), showing the presence of mesopore with a size distribution mainly ranging from 2 to 10 nm. (c) Thermogravimetric analysis of the as-dried monolith in air, showing an increase in the weight above 380 °C due to the oxidation of Si-H to Si-O. No PEO remains in the monolith after washing and drying. (d)  $^{29}\text{Si}$  solid-state CP-MAS NMR spectrum of the HSQ monolith, showing the presence of T<sup>3</sup> and T<sup>2</sup> signals, and the absence of Q signals. This evidences the total preservation of Si-H moiety throughout the process. (e) Scanning electron microscope images of as-dried HSQ monolith, showing the presence of well-defined macroporous co-continuous structure. (f) Digital camera image of a column-shaped HSQ monolith with 5 cm in length and 0.5 cm in diameter.

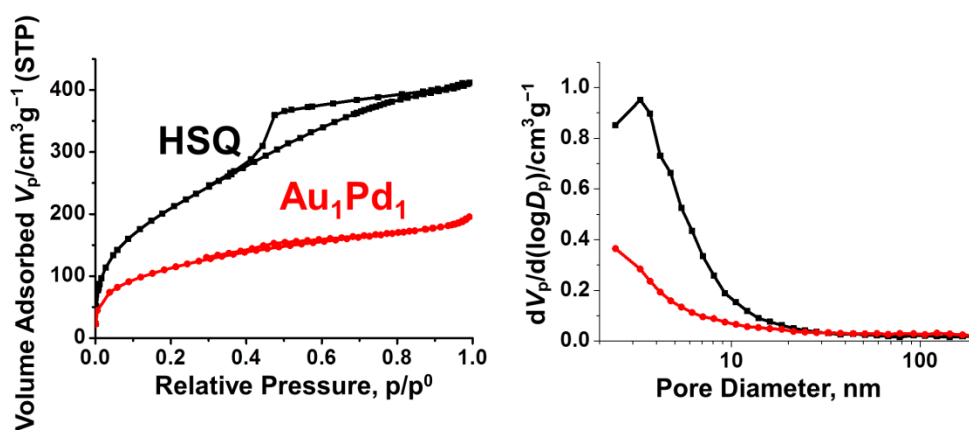


**Figure S2** Nitrogen adsorption-desorption isotherms (left) and the BJH pore size distributions (right) of the original HSQ and the Au<sub>1</sub>Pd<sub>1</sub>-supported HSQ.

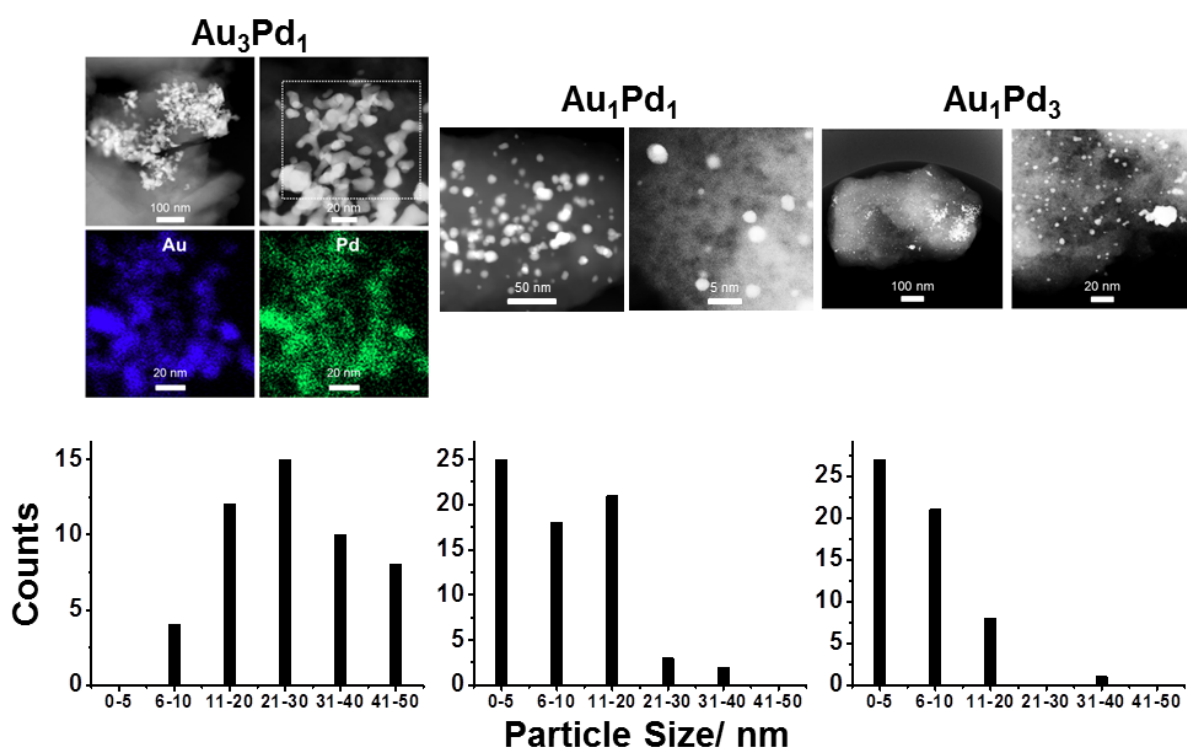


**Figure S3** (Top) HAADF-STEM images and EDS mapping of Au<sub>3</sub>Pd<sub>1</sub>, Au<sub>1</sub>Pd<sub>1</sub> and Au<sub>1</sub>Pd<sub>3</sub>, (bottom) particle size distributions of Au<sub>1</sub>Pd<sub>3</sub>, Au<sub>1</sub>Pd<sub>1</sub> and Au<sub>1</sub>Pd<sub>3</sub> (left to right).

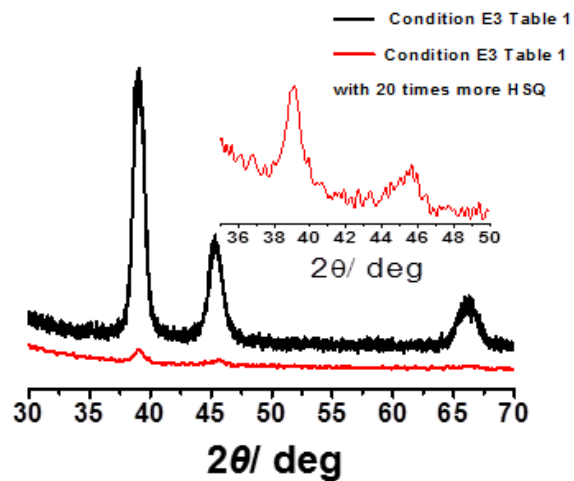


**Figure S4** Formation of  $\text{Au}_1\text{Pd}_1$  supported nanoparticles in the presence of 1 mmol (53 mg) and 20 mmol (1060 mg) of HSQ in the reaction system (E3 in Table 1), yielding 4 mol% and 0.2 mol% loaded  $\text{Au}_1\text{Pd}_1$  nanoparticles.

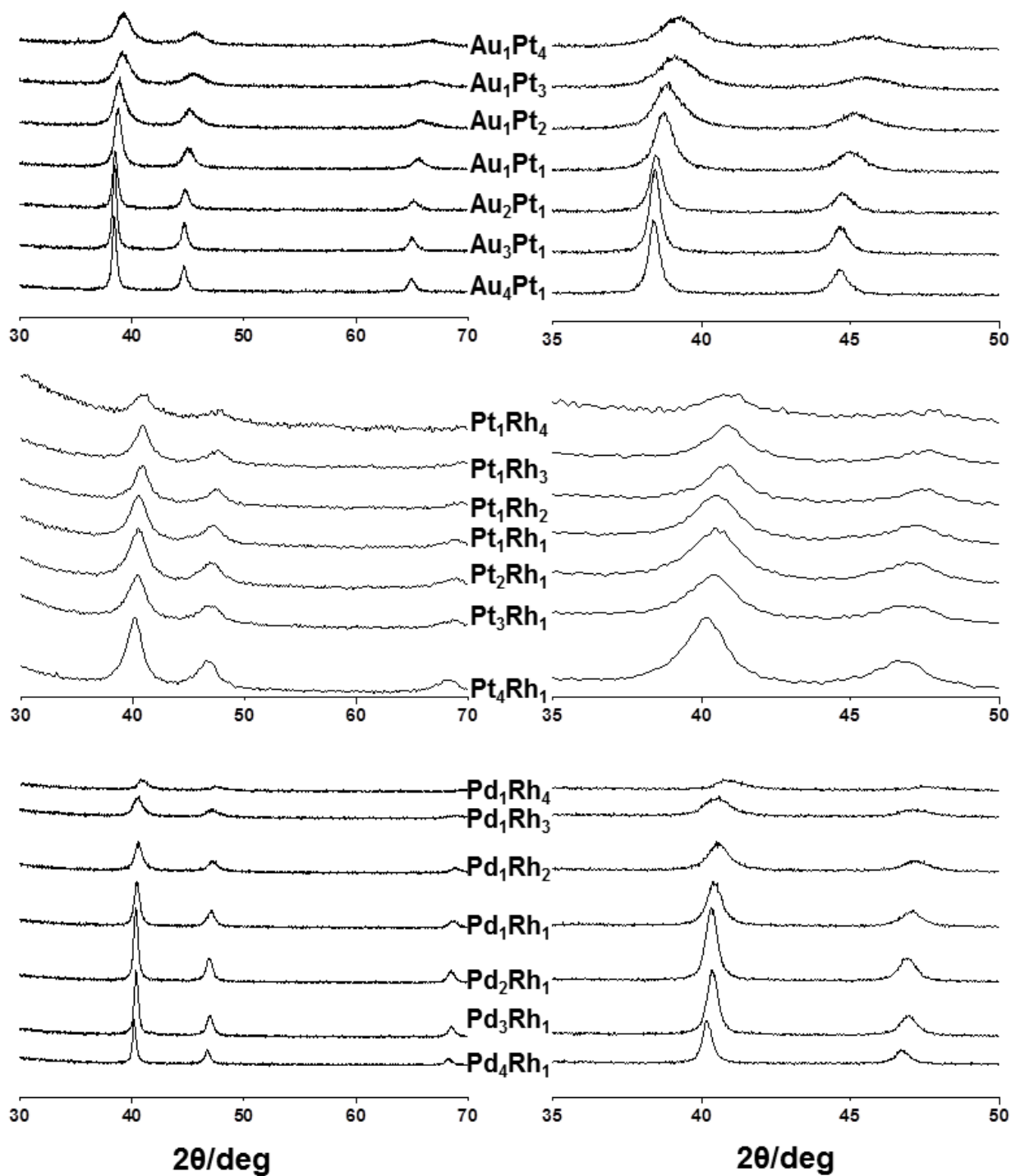


**Figure S5** X-ray diffraction patterns of HSQ monoliths embedded with bimetallic nanoparticles synthesized in different compositions.

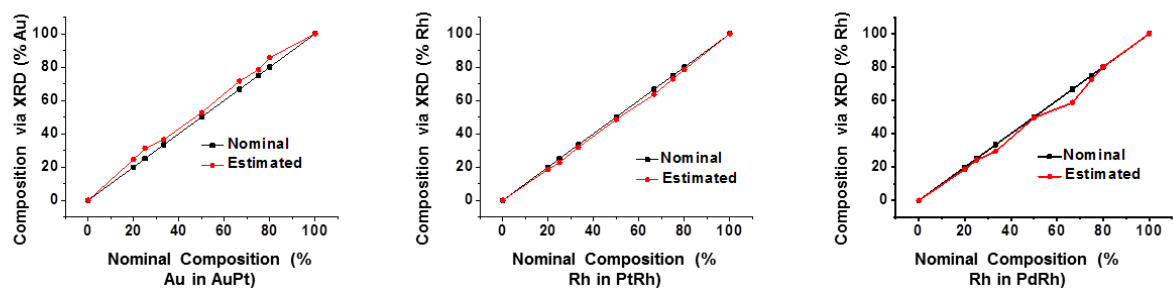


**Figure S6** Colleration of nominal and estimated (derived from Vegard's law) compositions of immobilized nanoparticles.

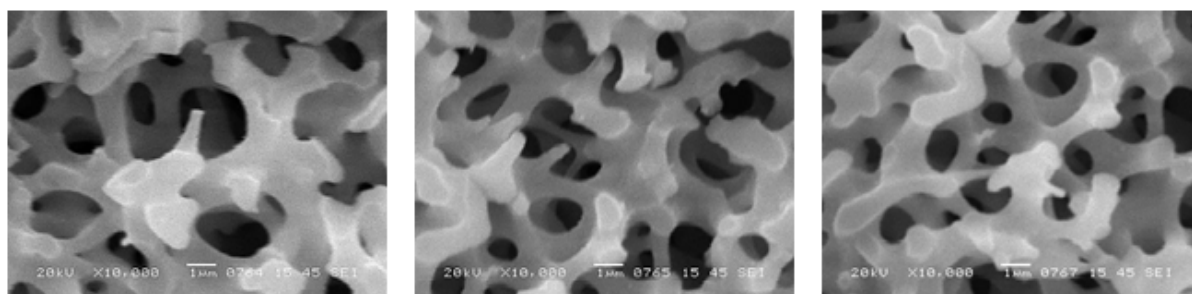


**Figure S7** SEM images of the HSQ monoliths embedded with Au<sub>1</sub>Pt<sub>1</sub> (left), Pt<sub>1</sub>Rh<sub>1</sub> (middle) and Pd<sub>1</sub>Rh<sub>1</sub> (right).

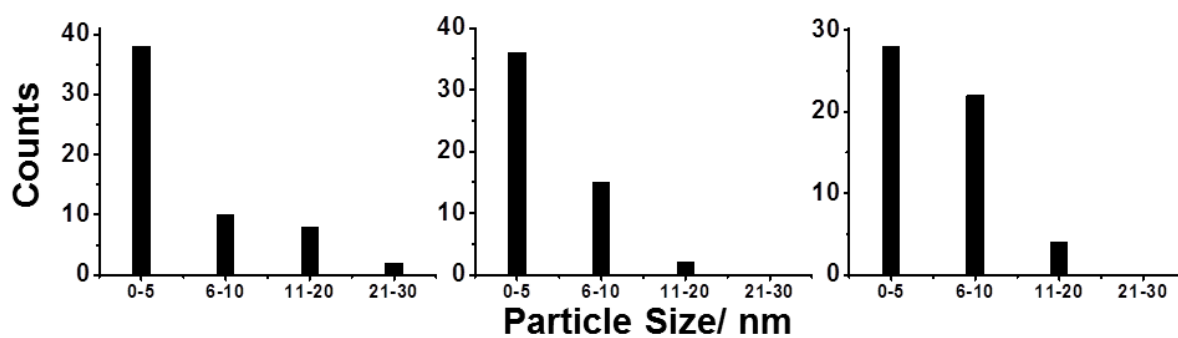


**Figure S8** Particle size (in nm) distributions of Au<sub>1</sub>Pt<sub>1</sub> (left), Pt<sub>1</sub>Rh<sub>1</sub> (middle) and Pd<sub>1</sub>Rh<sub>1</sub> (right) derived from HAADF-STEM images.

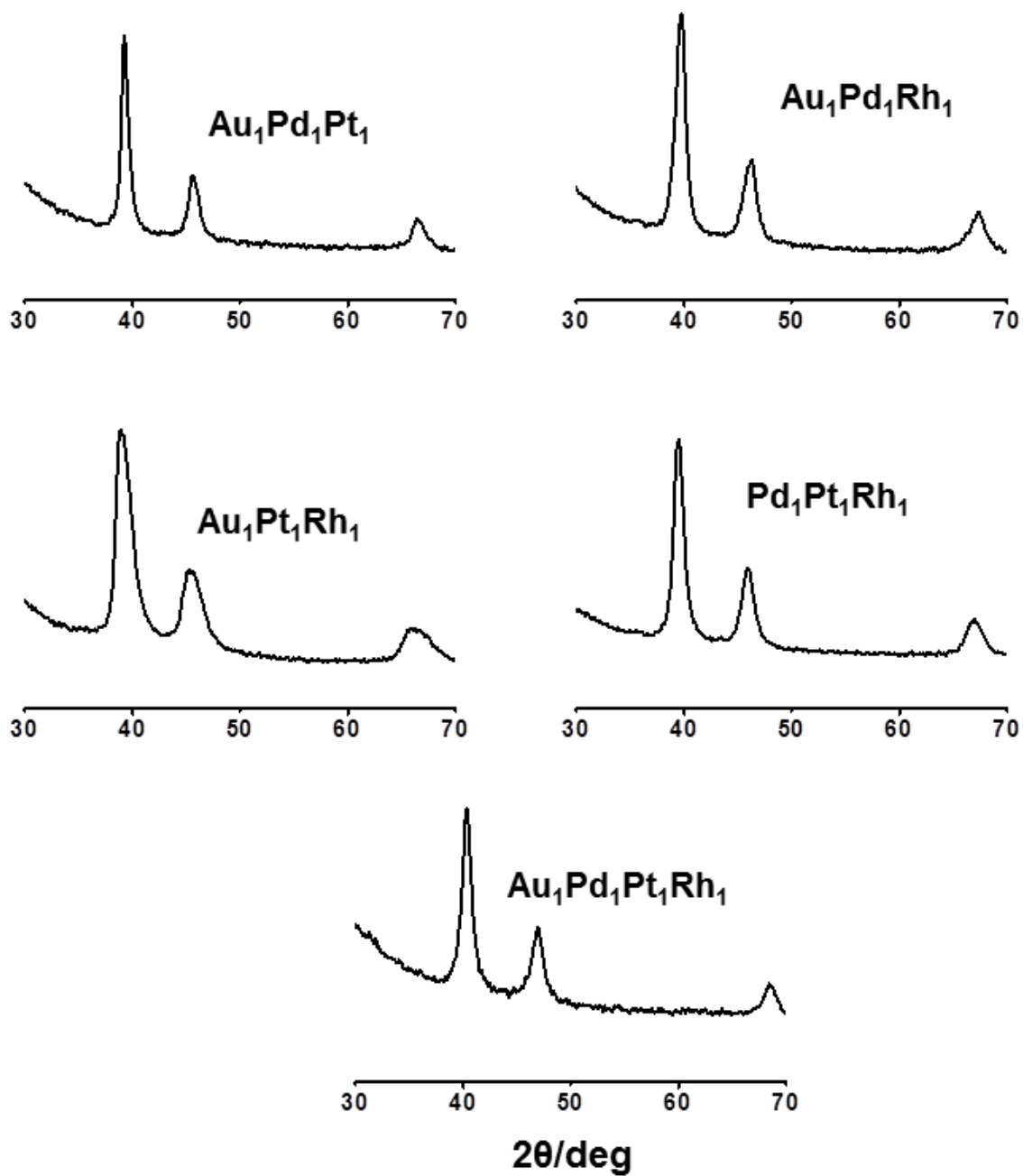


**Figure S9** X-ray diffraction patterns of the multimetallic nanoparticles immobilized on HSQ.

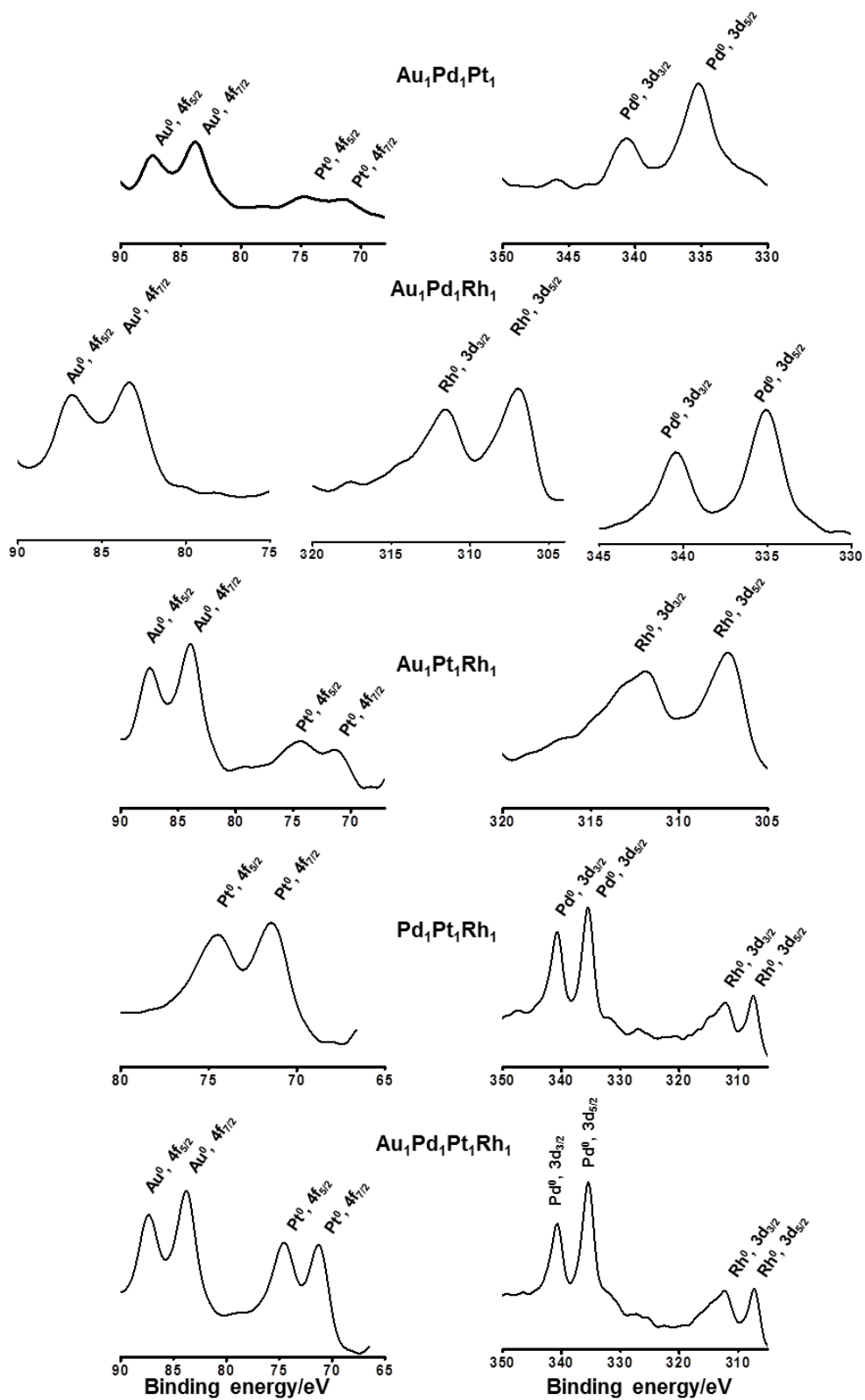


**Figure S10** XPS spectra of the multimetallic nanoparticles immobilized on HSQ.

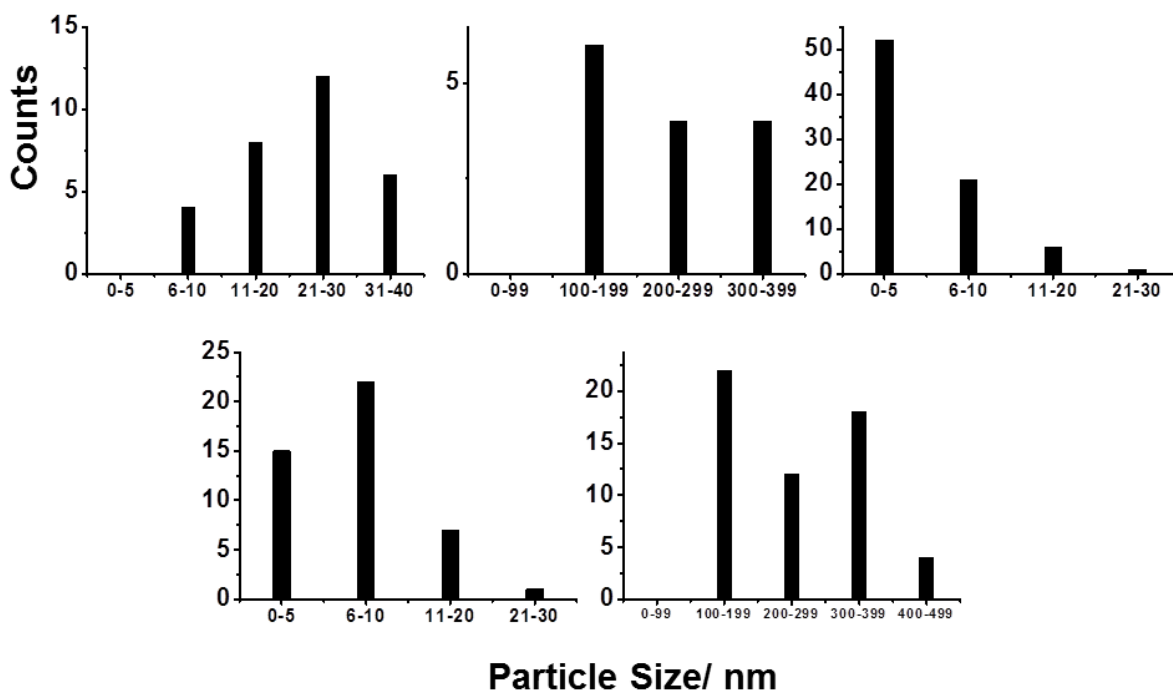


**Figure S11** Particle size (in nm) distributions of Au<sub>1</sub>Pd<sub>1</sub>Pt<sub>1</sub> (top left), Au<sub>1</sub>Pd<sub>1</sub>Rh<sub>1</sub> (top middle), Au<sub>1</sub>Pt<sub>1</sub>Rh<sub>1</sub> (top right), Pd<sub>1</sub>Pt<sub>1</sub>Rh<sub>1</sub> (bottom right) and Au<sub>1</sub>Pd<sub>1</sub>Pt<sub>1</sub>Rh<sub>1</sub> (bottom right) immobilized on HSQ.

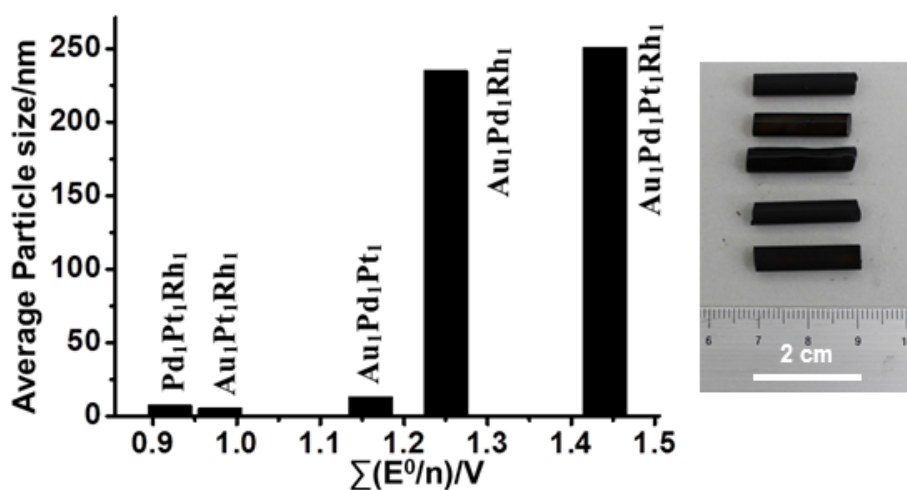


**Figure S12** (left) Relationship between average particle size and  $\sum(E^0/n)$  (an empirical parameter of  $E^0$  and oxidation number  $n$ ) in tri- and tetrametallic nanoparticles immobilized on HSQ. (right) Digital camera image of the monoliths embedded with Au<sub>1</sub>Pd<sub>1</sub>Pt<sub>1</sub>, Au<sub>1</sub>Pd<sub>1</sub>Rh<sub>1</sub>, Au<sub>1</sub>Pt<sub>1</sub>Rh<sub>1</sub>, Pd<sub>1</sub>Pt<sub>1</sub>Rh<sub>1</sub>, and Au<sub>1</sub>Pd<sub>1</sub>Pt<sub>1</sub>Rh<sub>1</sub> (from top to bottom) nanoparticles.

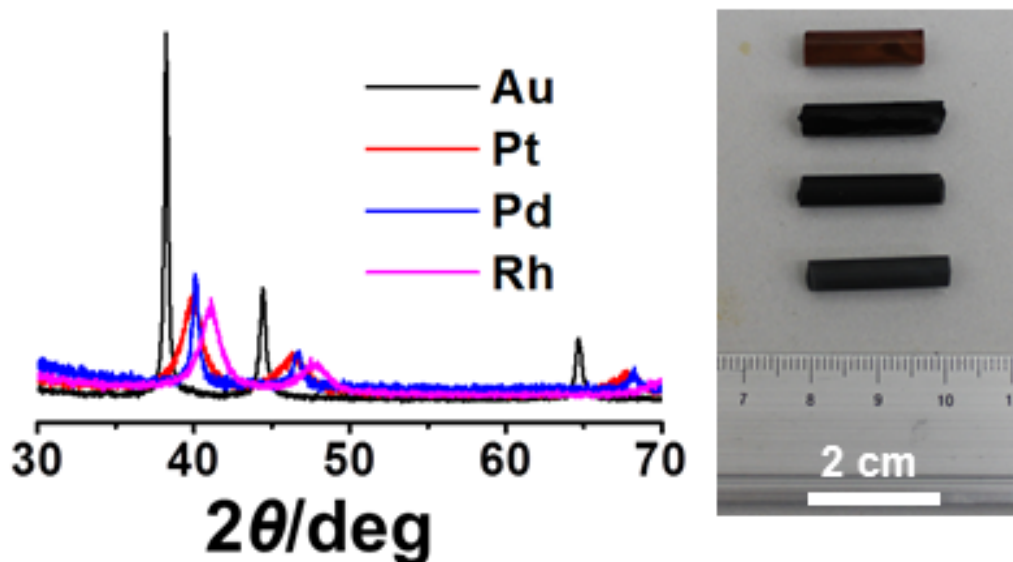


**Figure S13** X-ray diffraction patterns of HSQ-supported monometallic nanoparticles synthesized at 4 mol% loading (left). Digital camera image of Au, Pd, Pt and Rh (top to bottom) nanoparticle-embedded monoliths (right).

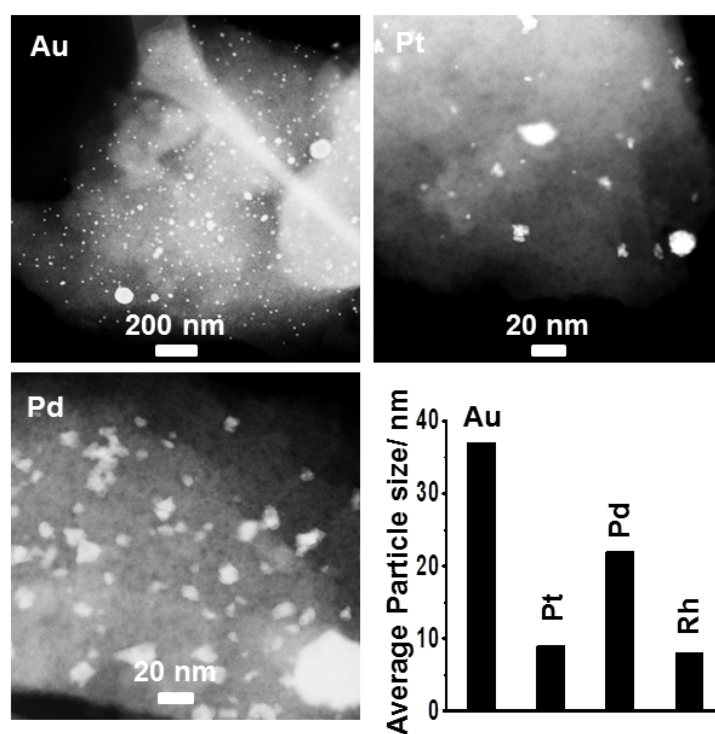


**Figure S14** HAADF-STEM images of Au, Pt and Pd nanoparticles embedded in HSQ. Average particle size was derived from XRD using the Scherrer's equation.

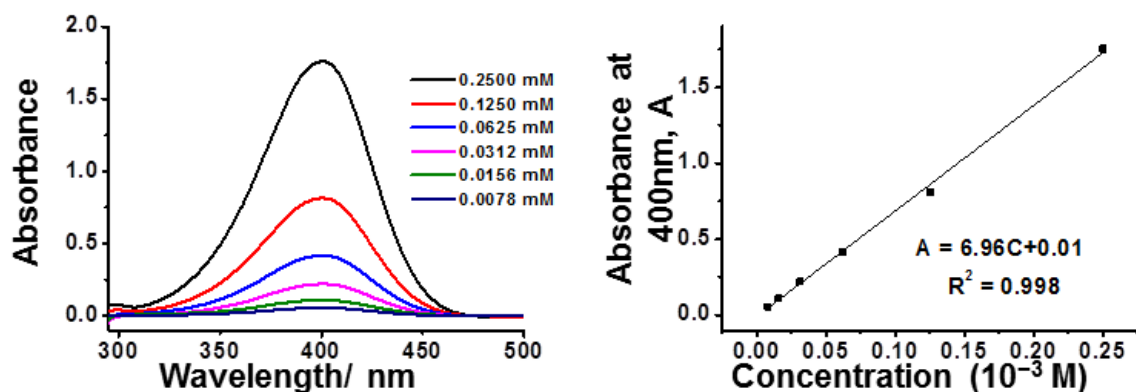


**Figure S15** Absorption spectra of mixture solutions of 4-NP and NaBH<sub>4</sub> in water-methanol (1:1) at different concentrations of 4-NP (left). Plot of absorbance at 400 nm against the concentration of 4-NP (right).

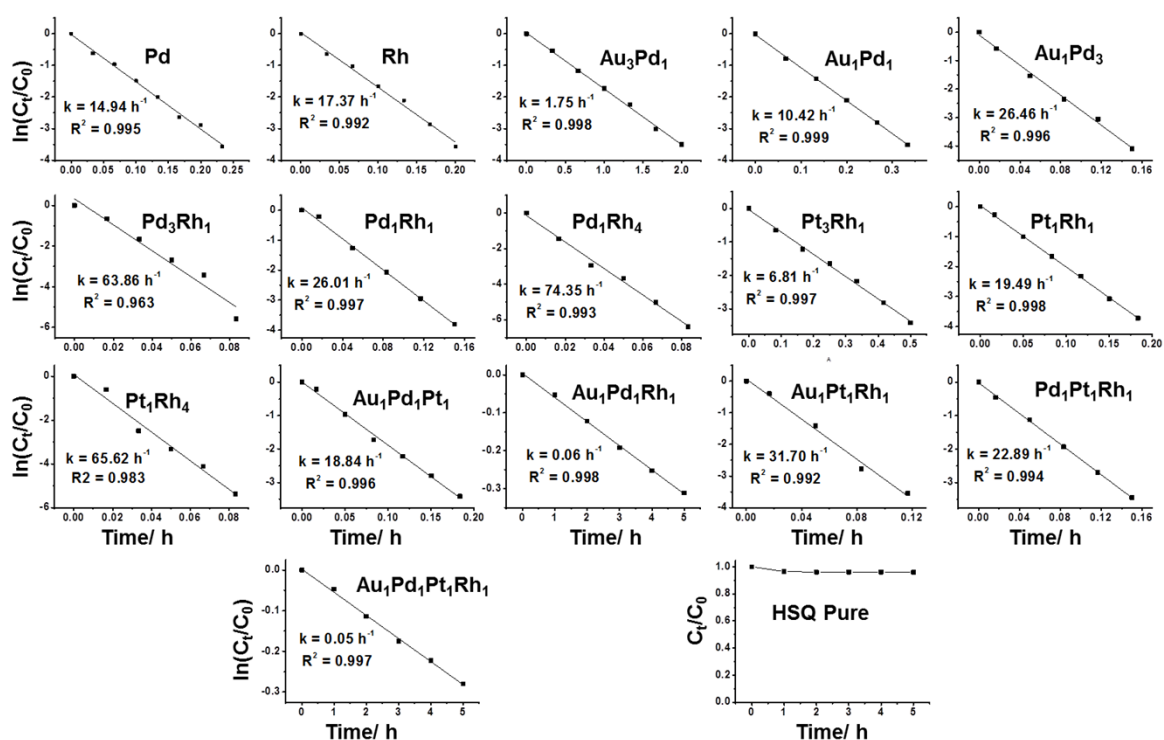


**Figure S16** Kinetics of catalytic reduction of 4-NP using nanoparticles supported on HSQ as the catalyst.

**Table S2** TOF and rate constant ( $k$ ) values in the reduction of 4-NP with different metal alloy nanoparticle-loaded HSQ monoliths as the catalyst.

Catalyst	TOF/h <sup>-1</sup>	$k$ /h <sup>-1</sup>	Catalyst	TOF/h <sup>-1</sup>	$k$ /h <sup>-1</sup>
HSQ	0	0	Pd <sub>4</sub> Rh <sub>1</sub>	2807.7	37.88
Au	14.0	0.14	Pd <sub>3</sub> Rh <sub>1</sub>	3926.8	63.86
Pd	1132.2	14.94	Pd <sub>2</sub> Rh <sub>1</sub>	2602.7	34.15
Pt	55.7	0.56	Pd <sub>1</sub> Rh <sub>1</sub>	2109.7	26.01
Rh	1507.8	17.37	Pd <sub>1</sub> Rh <sub>2</sub>	2163.8	26.85
Au <sub>4</sub> Pd <sub>1</sub>	22.0	0.22	Pd <sub>1</sub> Rh <sub>3</sub>	3322.7	48.47
Au <sub>3</sub> Pd <sub>1</sub>	172	1.75	Pd <sub>1</sub> Rh <sub>4</sub>	4258.0	74.35
Au <sub>2</sub> Pd <sub>1</sub>	320.1	3.29	Pt <sub>4</sub> Rh <sub>1</sub>	162.7	1.65
Au <sub>1</sub> Pd <sub>1</sub>	956.4	10.42	Pt <sub>3</sub> Rh <sub>1</sub>	643.7	6.81
Au <sub>1</sub> Pd <sub>2</sub>	1520.5	17.54	Pt <sub>2</sub> Rh <sub>1</sub>	963.1	10.50
Au <sub>1</sub> Pd <sub>3</sub>	2138.8	26.46	Pt <sub>1</sub> Rh <sub>1</sub>	1661.4	19.49
Au <sub>1</sub> Pd <sub>4</sub>	1120.6	13.65	Pt <sub>1</sub> Rh <sub>2</sub>	2276.1	30.27
Au <sub>4</sub> Pt <sub>1</sub>	26.0	0.26	Pt <sub>1</sub> Rh <sub>3</sub>	3202.1	45.82
Au <sub>3</sub> Pt <sub>1</sub>	77.5	0.78	Pt <sub>1</sub> Rh <sub>4</sub>	3986.0	65.62
Au <sub>2</sub> Pt <sub>1</sub>	132	1.34	Au <sub>1</sub> Pd <sub>1</sub> Pt <sub>1</sub>	1616.4	18.84
Au <sub>1</sub> Pt <sub>1</sub>	193.0	1.97	Au <sub>1</sub> Pd <sub>1</sub> Rh <sub>1</sub>	6.0	0.06
Au <sub>1</sub> Pt <sub>2</sub>	221.8	2.26	Au <sub>1</sub> Pt <sub>1</sub> Rh <sub>1</sub>	2461.3	31.7
Au <sub>1</sub> Pt <sub>3</sub>	256.9	2.61	Pd <sub>1</sub> Pt <sub>1</sub> Rh <sub>1</sub>	1902.3	22.89
Au <sub>1</sub> Pt <sub>4</sub>	117.8	1.19	Au <sub>1</sub> Pd <sub>1</sub> Pt <sub>1</sub> Rh <sub>1</sub>	5.0	0.05

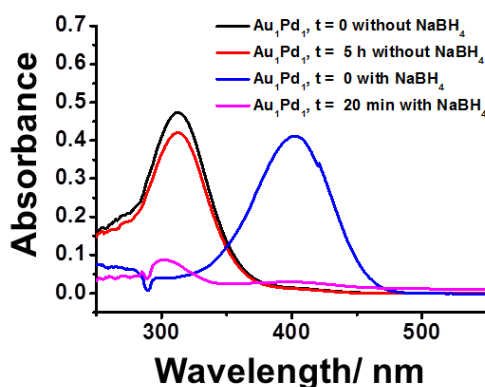


**Figure S17** Reduction of 4-NP with and without using NaBH<sub>4</sub> as the reducing agent in the presence of Au<sub>1</sub>Pd<sub>1</sub>-embedded HSQ as the catalyst. Since no deprotonation of 4-NP occurs without NaBH<sub>4</sub>, the maximum absorbance of 4-NP locates at 310 nm. However, in the presence of NaBH<sub>4</sub>, deprotonation of 4-NP occurs, showing the maximum absorbance at 400 nm. It can be confirmed that the rapid catalytic reduction proceeds under the presence of NaBH<sub>4</sub>, while virtually no reduction is observed without NaBH<sub>4</sub>.

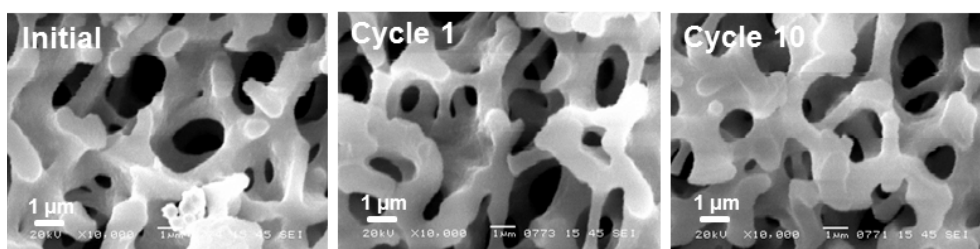


**Figure S18** SEM images of the Pd<sub>1</sub>Rh<sub>4</sub> nanoparticle-embedded monolith before and after using it as the catalyst for 4-NP reduction, showing preservation of macroporous co-continuous structure of the support HSQ even after the 10th catalytic cycle.

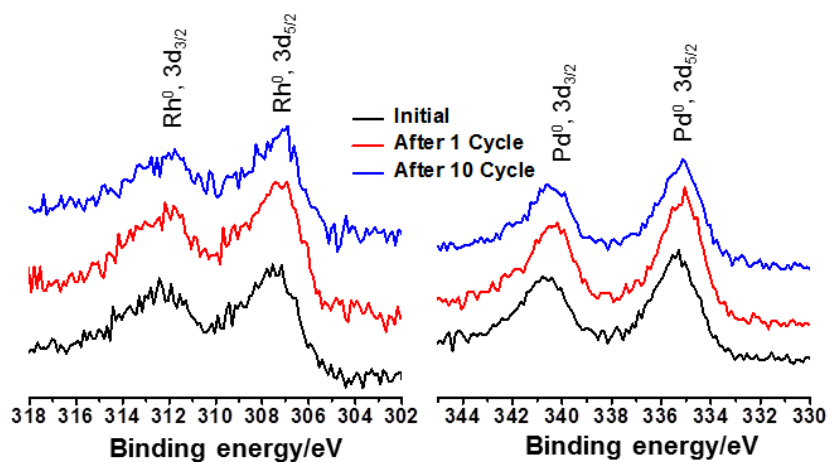


**Figure S19** XPS results of the Pd<sub>1</sub>Rh<sub>4</sub> nanoparticle-embedded monolith before and after using it as the catalyst, showing no change in the both element after 10 cycles.

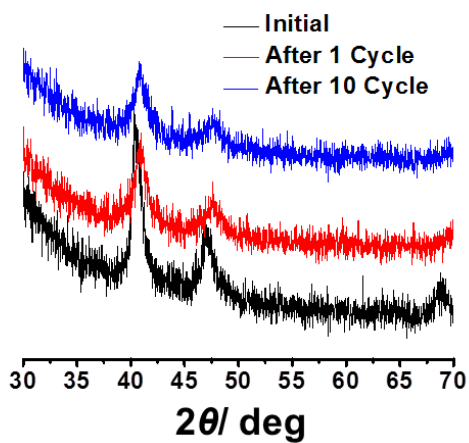


**Figure S20** XRD of the Pd<sub>1</sub>Rh<sub>4</sub> nanoparticle-embedded monolith before and after using it as the catalyst.